Proceedings of the 2007 American Control Conference
Marriott Marquis Hotel at Times Square
New York City, USA, July 11-13, 2007



# $\mathcal{L}_1$ Adaptive Controller for Tailless Unstable Aircraft

Vijay V. Patel, Chengyu Cao, Naira Hovakimyan, Kevin A. Wise and Eugene Lavretsky

*Abstract*— **The advantages of $\mathcal{L}_1$ adaptive control architecture, such as improved transient and asymptotic tracking, guaranteed time-delay margin achieved via smooth control input, have been previously established. In this paper, the $\mathcal{L}_1$ adaptive controller is designed for a multi-input multi-output open loop unstable unmanned military aircraft. The control is designed to accommodate and to be robust to actuator failures, as well as to pitch break uncertainty that is used to model uncertain aerodynamics. Results of using the $\mathcal{L}_1$ adaptive controller are compared with the conventional model reference adaptive control scheme to show improved transient command tracking and time-delay margin.**

## I. Introduction

Since the early 1990's, the Air Force, Navy, and NASA working with industry and academia have made significant progress towards maturing adaptive control theory for application to reconfigurable/damage adaptive flight control for aircraft and weapon systems [1]–[13]. Reconfigurable flight control refers to the ability of a flight control system to adapt to unknown failures, damage, and uncertain aerodynamics. Flight control systems that are reconfigurable and damage adaptive constitute an important element in the design of mission effective unmanned combat systems. Moreover, these architectures play an important role in increasing the reliability of unmanned systems. Both indirect and direct adaptive control methods have been investigated, and several different approaches have been successfully flown on manned aircraft [1]–[4], unmanned aircraft [5], [6], and also on advanced weapon systems [10]–[12].

The Self Designing Controller [1] program successfully flight tested an indirect adaptive scheme on the VISTA/F-16 aircraft which used least squares system identification, with spatial and temporal constraints, to estimate the stability and control derivatives required for the solution of a receding horizon optimal control problem. NASA [2] has also tested both an indirect and direct adaptive method on an F-15 aircraft. The indirect method used neural network based system identification algorithms to estimate aircraft plant matrices and sent these to an online Riccati equation solver. Kim and Calise [4] presented an approach based on neural networks for a feedback linearizing control architecture and demonstrated the approach via simulation studies with an F/A-18 aircraft. This approach was later modified and used in the Reconfigurable Control for Tailless Fighters (RESTORE) program [4]–[6], using a dynamic inversion control law in an explicit model following framework. The successful application of this technology under the RESTORE program [6] led to the flight testing of the approach on the Boeing/NASA X-36 Agility Research Test Aircraft. NASA has also been flight testing a similar approach on their F-15 aircraft. This same approach also has been applied and flown on the Joint Direct Attack Munition (JDAM) [10], [12]–[14], in which the LQR based flight control system was replaced with a dynamic inversion based scheme augmented with a neural-network based model reference adaptive control. A historical overview of research on reconfigurable flight control is available in [15].

In [16], Lavretsky and Wise applied model reference adaptive control (MRAC) to a model of the aerodynamically unstable X-45A UCAV. Although successful, implementation of the adaptive control proved to be sensitive to the size of the learning rate, requiring numerical simulations to validate robustness to time-delays. Other open problems regarding the application of MRAC control to aircraft have been documented in [17].

This paper presents application of $\mathcal{L}_1$ adaptive control from [18], [19], [22] to the unmanned military aircraft model from [16]. In [16], the adaptive control architecture includes a baseline inner loop control which is augmented by an online feedforward neural network. The baseline inner loop control provides nominal system performance, while the adaptive increment accommodates unknown/unexpected control failures and model uncertainties. The approach in this paper extends the results of [16] to a new class of adaptive controllers, known as $\mathcal{L}_1$ adaptive controllers. The benefit of $\mathcal{L}_1$ adaptive controller is its ability of fast and robust adaptation that leads to desired transient performance for system's both signals, input and output, simultaneously. Moreover, for open-loop systems linearly depending upon unknown parameters, the (nonlinear) $\mathcal{L}_1$ adaptive controller has analytically computable stability margins [21]. In the case of open-loop nonlinear systems, as the one considered in this paper, the margins are computed numerically based on simulations. However, the insights are based on the results of [21], which relate the time-delay margin to the underlying filter of $\mathcal{L}_1$ adaptive controller.

The paper is organized as follows. Section II gives the problem formulation. In Section III, the novel $\mathcal{L}_1$ adaptive control architecture is presented. Stability and uniform transient tracking bounds of $\mathcal{L}_1$ adaptive controller are presented

This material is based upon work supported by the United States Air Force under Contracts No. FA8650-05-C-3563, FA9550-05-1-0157, FA9550-04-C-0047 and ONR under Contract N00014-05-1-0828. Any opinions, findings and conclusions or recommendations expressed in this material are those of the authors and do not necessarily reflect the views of the United States Air Force and ONR.

V. Patel, C. Cao, N. Hovakimyan are with Aerospace & Ocean Engineering, Virginia Polytechnic Institute & State University, Blacksburg, VA 24061-0203, e-mail: {vvp2069, chengyu, nhovakim}@vt.edu; K. Wise and E. Lavretsky are with the Boeing Co., e-mail: {kevin.a.wise, eugene.lavretsky}@boeing.com

1-4244-0989-6/07/$25.00 ©2007 IEEE.

in Section III-A. In section IV, simulation results are presented, while Section V concludes the paper.

## II. Problem Formulation

Following [16], we present aircraft dynamics as

$$\dot{x}(t) = Ax(t) + B_1\Lambda\left(\delta(t) + K_0(x_p(t))\right) + B_2u(t)\,, \quad (1)$$

where $x(t) \in R^9, \delta(t) \in R^3$ (virtual control input), $u(t) \in R^4$ are the measured system states, control signals and reference inputs, respectively, $A \in R^{9\times9}$, $B_1 \in R^{9\times3}$, $B_2 \in R^{9\times4}$ are known matrices, $\Lambda$ is unknown constant positive diagonal matrix of appropriate dimension. The state vector $x = (\alpha, \beta, p, q, r, q_I, p_I, r_I, r_w)^\top$ comprises five of plant states ($x_p$), which include angle of attack $\alpha$, angle of sideslip $\beta$, body roll rate $p$, body pitch rate $q$, body yaw rate $r$ and four baseline controller ($x_c$) states, which include pitch integrator $q_I$, roll integrator $p_I$, yaw integrator $r_I$, and yaw rate washout filter signal $r_w$. The vector $u = (a_z^{cmd}, \beta^{cmd}, p^{cmd}, r^{cmd})^\top$ consists of four inner loop commands i.e., vertical acceleration $a_z^{cmd}$, sideslip $\beta^{cmd}$, roll rate $p^{cmd}$ and yaw rate $r^{cmd}$, and $\delta$ is a vector of virtual controls (roll, pitch and yaw control).

Note that the vector-function $K_0(x_p)$ represents matched unknown nonlinear effects. In addition to unknown $K_0(x_p)$, $\Lambda$ models actuator failures and loss of control effectiveness. The inner-loop control objective is to design a full state-feedback controller $\delta(t)$ for (1) such that all closed-loop signals remain bounded and the system state tracks the state of a desired reference model.

## III. $\mathcal{L}_1$ Adaptive controller

Consider the following control law

$$\delta(t) = \delta_L(t) + \delta_{ad}(t), \quad (2)$$

where $\delta_L(t)$ is the component of the baseline linear controller, and $\delta_{ad}(t)$ is the adaptive increment. Feedback/feedforward gains for the baseline (nominal) inner-loop controller are designed in [16] assuming no modeling uncertainties, (i.e., $\Lambda = I_3$ and $K_0(x_p) = 0_{3\times1}$) using the robust servomechanism LQR method with output projection ( [23], [24] and [25]). The corresponding inner-loop control system takes the form:

$$\delta_L(t) = K_x^\top x(t) + K_u^\top u(t)\,, \quad (3)$$

where $K_x$ and $K_u$ denote the $(9\times3)$ and $(4\times3)$ - nominal feedback and feedforward gain matrices, correspondingly. Nominal inner loop feedback when applied to the ideal model (1) (i.e. without uncertainties), leads to

$$A_m = A + B_1K_x^\top, \quad B_m = B_2 + B_1K_u^\top, \quad (4)$$

which characterize the desired transient and steady state response for a given reference input $u(t)$:

$$\dot{x}_m(t) = A_mx_m(t) + B_mu(t)\,. \quad (5)$$

We note that the choice of $K_x$ and $K_u$ has to render $A_m$ Hurwitz and and provide unity DC gains from the commanded signals to the corresponding system outputs.

Using the stabilizing gains for the inner-loop, the system in (1) takes the form:

$$\dot{x}(t) = (A + B_1\Lambda K_x^T)x(t) + B_1\Lambda(\delta_{ad} + K_0(x_p)) + (B_2 + B_1\Lambda K_u^T)u(t)\,. \quad (6)$$

From (4) and (6), we have

$$\dot{x}(t) = A_mx(t) + B_mu(t) + B_1\Lambda\Big(\delta_{ad}(t) + K_1(x(t), u(t))\Big)\,, \quad (7)$$

where

$$\begin{aligned} K_1(x(t), \sigma(t)) &= K_0(x_p(t)) + \theta^\top x(t) + \sigma(t)\,, \\ \theta^\top &= -\Lambda^{-1}(I-\Lambda)K_x^\top\,, \\ \sigma(t) &= -\Lambda^{-1}(I-\Lambda)K_u^\top u(t)\,. \end{aligned} \quad (8)$$

We note that, given a compact set $\mathcal{D}$, the nonlinearity $K_0(x_p)$ can be approximated using a feedforward neural network (NN):

$$K_0(x_p) = W^\top\Phi(x_p) + \epsilon(x_p)\,, \quad (9)$$

where $W \in R^{N_0\times3}$ is a matrix of unknown parameters that belongs to a known (conservative) compact set $W \in \mathcal{W}$, $\Phi(x_p)$ is a vector of suitably chosen RBFs, $||\epsilon(x_p)|| \le \epsilon^*$ is the uniformly bounded approximation error on $\mathcal{D}$. We further assume that

$$\theta \in \Theta\,, \quad \|\sigma(t)\| \le \Delta\,, \quad \|\dot{\sigma}(t)\| \le d_\Delta\,, \quad \forall\ t \ge 0\,, \quad (10)$$

where $\Theta$ is a known compact set, $\Delta$, $d_\Delta$ are known conservative bounds. Next, we introduce the elements of the $\mathcal{L}_1$ neural adaptive controller.

**State Predictor Model:**

$$\dot{\hat{x}}(t) = A_m\hat{x}(t) + B_mu(t) + B_1\Big(\delta_{ad}(t) + \hat{\theta}^\top(t)x(t) + \hat{W}^\top(t)\Phi(x_p(t)) + \hat{\sigma}(t)\Big)\,, \quad (11)$$

in which $\hat{\theta}(t), \hat{W}(t), \hat{\sigma}(t)$ are the adaptive parameters.

**Adaptive Laws:**

$$\begin{aligned} \dot{\hat{W}}(t) &= \mathrm{Proj}(\hat{W}(t), -\Phi(x_p(t))\tilde{x}^\top(t)PB_1\Gamma_W)\,, \\ \dot{\hat{\theta}}(t) &= \mathrm{Proj}(\hat{\theta}(t), -x(t)\tilde{x}^\top(t)PB_1\Gamma_\theta)\,, \\ \dot{\hat{\sigma}}(t) &= \mathrm{Proj}(\hat{\sigma}(t), -\Gamma_\sigma(\tilde{x}^\top(t)PB_1)^\top)\,, \end{aligned} \quad (12)$$

in which $\tilde{x}(t) = \hat{x}(t) - x(t)$ is the tracking error between the system dynamics in (1) and the state predictor in (11), $\Gamma_W = \Gamma_\theta = \Gamma_\sigma = \Gamma_cI_{3\times3}$ are the matrices of adaptations gains, and $P = P^\top > 0$ is the solution of the algebraic Lyapunov equation $A_m^\top P + PA_m = -Q$, $Q > 0$, while $\mathrm{Proj}(\cdot,\cdot)$ denotes the projection operator [26].

**Control Law:** The adaptive control signal is defined as the output of a stable filter:

$$\delta_{ad}(s) = C(s)\bar{r}(s)\,, \quad (13)$$

where $\bar{r}(s)$ is the Laplace transformation of $\bar{r}(t) = -\hat{W}^\top(t)\Phi(x_p(t)) - \hat{\theta}^\top(t)x(t) - \hat{\sigma}(t)$, and

$$C(s) = \begin{bmatrix} C_1(s) & 0 & 0 \\ 0 & C_2(s) & 0 \\ 0 & 0 & C_3(s) \end{bmatrix} \quad (14)$$

with $C_1(s)$, $C_2(s)$ and $C_3(s)$ being strictly proper stable systems with unit low-pass gain: $C_1(0) = C_2(0) = C_3(0) = 1$. A simple choice is to select

$$C_1(s) = C_2(s) = C_3(s) = \frac{\omega_a}{s+\omega_a}\,, \tag{15}$$

where $\omega_a$ indicates the bandwidth of the filter. Let $L$ be a conservative bound for the Lipchitz constant of the uncertainty $K_0(x_p)$ in (9) on the compact set $\mathcal{D}$, i.e. there exist $L$ and $L_0$ such that

$$\begin{aligned} |K_0(0)|_\infty &\leq L_0\,, \\ |K_0(x_{p1}) - K_0(x_{p2})|_\infty &\leq L\|x_{p1} - x_{p2}\|_\infty\,. \end{aligned} \tag{16}$$

**$\mathcal{L}_1$-gain requirement:** Design $C(s)$ to satisfy

$$\|\bar{G}(s)\|_{\mathcal{L}_1} < \frac{1}{(L+L_1)}\,, \tag{17}$$

where

$$\begin{aligned} L_1 &= \max_{\theta\in\Theta}\|\theta^\top\|_{\mathcal{L}_1}\,, \\ \bar{G}(s) &= (sI - A_m)^{-1}B_1(C(s)-1)\,. \end{aligned} \tag{18}$$

Let $W_{\max} \triangleq \max_{W\in\mathcal{W}} 4\|W\|^2 + \max_{\theta\in\Theta} 4\|\theta\|^2, G(s) = (sI - A_m)^{-1}B_m, H_o(s) = (sI - A_m)^{-1}B_1$. The compact set $\mathcal{D}$ of the RBF distribution is defined as

$$\mathcal{D} = \{x \,|\, \|x\|_\infty < \gamma_r + \gamma_1 + \gamma_0\}, \tag{19}$$

where

$$\gamma_r = \frac{\|G(s)\|_{\mathcal{L}_1}\|u\|_{\mathcal{L}_\infty} + \|\bar{G}(s)\|_{\mathcal{L}_1}(L_0+\epsilon^*+\Delta) + \|H_o(s)\|_{\mathcal{L}_1}\epsilon^*}{1-\|\bar{G}(s)\|_{\mathcal{L}_1}(L+L_1)} \tag{20}$$

$$\gamma_0 = \sqrt{\frac{\lambda_{\max}(P)}{\lambda_{\min}(P)}\left(\frac{2\|PB_1\|}{\lambda_{\min}(Q)}\left(\epsilon^* + \frac{d\Delta}{\Gamma_c}\right)\right)^2 + \frac{W_{\max}}{\lambda_{\min}(P)\lambda_{\min}(\Lambda)\Gamma_c}} \tag{21}$$

$$\gamma_1 = \frac{5\epsilon^*\|\bar{G}(s)\|_{\mathcal{L}_1} + \|H_o(s)\|_{\mathcal{L}_1}\epsilon^* + (1+\|C(s)-1\|_{\mathcal{L}_1})\gamma_0}{1-\|\bar{G}(s)\|_{\mathcal{L}_1}(L+L_1)} \tag{22}$$

The $\mathcal{L}_1$ adaptive controller is defined via (11), (12), (13) subject to (17), with the RBF distribution set given in (19).

### A. Performance Analysis of the $\mathcal{L}_1$ Adaptive Controller

Consider the following closed-loop reference system:

$$\begin{aligned} \dot{x}_{ref}(t) &= A_m x_{ref}(t) + B_m u(t) + B_1\Lambda\Big(\delta_{ref}(t) \\ &\quad + K_0(x_{ref}(t)) + \theta^\top x(t) + \sigma(t)\Big)\,, \end{aligned} \tag{23}$$

where

$$\delta_{ref}(s) = -C(s)r_{ref}(s)\,, \tag{24}$$

and $r_{ref}(t) = K_0(x_p(t)) + \theta^\top x(t) + \sigma(t)$. For a diagonal and positive definite $\Lambda$, we define $\delta_m(t) = \Lambda^{-1}\delta_{ad}(t), \hat{W}_m(t) = \hat{W}(t)\Lambda^{-1}, \hat{\theta}_m(t) = \hat{\theta}(t)\Lambda^{-1}, \hat{\sigma}_m(t) = \Lambda^{-1}\hat{\sigma}(t), \Gamma_{Wm} = \Lambda^{-1}\Gamma_W, \Gamma_{\theta m} = \Lambda^{-1}\Gamma_\theta, \Gamma_{\sigma m} = \Lambda^{-1}\Gamma_\sigma$.

Hence, the $\mathcal{L}_1$ adaptive controller in (11), (12), (13) can be rewritten as:

$$\begin{aligned} \dot{\hat{x}}(t) &= A_m\hat{x}(t) + B_m u(t) + B_1\Lambda\Big(\delta_m(t) + \hat{\theta}_m^\top(t)x(t) \\ &\quad + \hat{W}_m^\top(t)\Phi(x_p(t)) + \hat{\sigma}_m(t)\Big)\,, \end{aligned} \tag{25}$$

$$\begin{aligned} \dot{\hat{W}}_m(t) &= \mathrm{Proj}(\hat{W}_m(t), -\Phi(x_p(t))\tilde{x}^\top(t)PB_1\Gamma_{Wm})\,, \\ \dot{\hat{\theta}}_m(t) &= \mathrm{Proj}(\hat{\theta}_m(t), -x(t)\tilde{x}^\top(t)PB_1\Gamma_{\theta m})\,, \\ \dot{\hat{\sigma}}_m(t) &= \mathrm{Proj}(\hat{\sigma}_m(t), -\Gamma_\sigma(\tilde{x}^\top(t)PB_1)^\top)\,, \end{aligned} \tag{26}$$

$$\delta_m(s) = C(s)\bar{r}_m(s)\,, \tag{27}$$

where $\bar{r}_m(s)$ is the Laplace transformation of $\bar{r}_m(t) = -\hat{W}_m^\top(t)\Phi(x_p(t)) - \hat{\theta}_m^\top(t)x(t) - \hat{\sigma}_m(t)$.

*Theorem 1:* [19], [22] Given the reference system in (23) and the system in (1) with $\mathcal{L}_1$ adaptive controller, defined via (11), (12), (13) subject to (17), we have:

$$\|x_{ref}\| \leq \gamma_r, \tag{28}$$

$$\|x - x_{ref}\|_{\mathcal{L}_\infty} \leq \gamma_1\,, \tag{29}$$

$$\|\delta_m - \delta_{ref}\|_{\mathcal{L}_\infty} \leq \gamma_2\,, \tag{30}$$

where

$$\gamma_2 = \left\| C(s)\begin{bmatrix} c_{o_1}^\top H_{o1}(s)) & 0 & 0 \\ 0 & c_{o_2}^\top H_{o3}(s)) & 0 \\ 0 & 0 & c_{o_3}^\top H_{o3}(s)) \end{bmatrix}^{-1} \begin{bmatrix} c_{o_1}^\top \\ c_{o_2}^\top \\ c_{o_3}^\top \end{bmatrix} \right\|_{\mathcal{L}_1} \gamma_0 + \|C(s)\|_{\mathcal{L}_1}(L+L_1)\gamma_1 + 3\|C(s)\|_{\mathcal{L}_1}\epsilon^*, \tag{31}$$

in which $c_{o_i} \in \mathbb{R}^9$ is a vector that renders $c_{o_i}^\top H_{o_i}(s)$ minimum phase with relative degree 1, $H_{o_i}(s)$ being the $i^{th}$ column of $H_o(s)$.

It follows from and (20), (21), (22) and (31) that

$$\lim_{\epsilon^*\to 0,\Gamma_c\to\infty}\gamma_0 = 0,\ \lim_{\epsilon^*\to 0,\Gamma_c\to\infty}\gamma_1 = 0,\ \lim_{\epsilon^*\to 0,\Gamma_c\to\infty}\gamma_2 = 0\,.$$

Hence, if the the approximation error of the RBF network is small enough, we can arbitrarily minimize the bounds between the signals of the closed-loop $\mathcal{L}_1$ adaptive system and the closed-loop reference system. Thus the problem is reduced to design of $C(s)$ to ensure that the closed-loop reference system in (23) approximates the response in (5). We note that the control law $\delta_{ref}(t)$ in the closed-loop reference system, which is used in the analysis of $\mathcal{L}_\infty$ norm bounds, is not implementable since its definition involves the unknown parameters. Theorem 1 ensures that the $\mathcal{L}_1$ adaptive controller approximates $\delta_{ref}(t)$ both in transient and steady state. So, it is important to understand how these bounds can be used for ensuring uniform transient response with *desired* specifications. We notice that the following *ideal* control signal $\delta_{ideal}(t) = -r_{ref}(t)$ is the one that cancels the uncertainties exactly leading to (5). In the closed-loop reference system (23), $\delta_{ideal}(t)$ is further low-pass filtered by $C(s)$ to have guaranteed low-frequency range. In [19], specific design guidelines are provided for selection of $C(s)$ to ensure that the reference system in (23) tracks the response

of the desired system in (5). One way to achieve this is via the selection of a strictly proper system $C(s)$ that minimizes the $\mathcal{L}_1$-gain of one of the cascaded system $C(s)(1-C(s))$. We also notice that for any finite $L$ the condition in (17) can always be satisfied by increasing the bandwidth of $C(s)$.

*Remark 1:* Notice that if we set $C(s) = 1$, then the $\mathcal{L}_1$ neural controller degenerates into a MRAC type. In that case $\left\| C_i(s)\frac{1}{c_{o_i}^\top H_{o_i}(s)} \right\|_{\mathcal{L}_1}$ cannot be finite for any $i = 1, 2, 3$, since $H_{o_i}(s)$ is strictly proper. Therefore, from (31) it follows that $\gamma_2 \to \infty$, and hence for the control signal in conventional MRAC type neural network adaptive controller one can not reduce the bound in (30) by increasing the adaptive gain.

*Remark 2:* Recall that in conventional MRAC scheme the ultimate bound is given by $\gamma_0$ defined in (21). Notice that $\gamma_0$ depends upon $\epsilon^*$, $W_{\max}$ and $\Gamma_c$. While $\epsilon^*$ and $W_{\max}$ are interconnected via the choice of RBFs, $\Gamma_c$ is a design parameter of the adaptive process that can be used to reduce the ultimate bound. However, increasing $\Gamma_c$ in the conventional MRAC scheme leads the control signal into high-frequency oscillations. With the $\mathcal{L}_1$ adaptive control architecture the ultimate bound of the tracking error is given by $\gamma_1$ in (29). From the definition of it in (22) it follows that $\gamma_1 > \gamma_0$. Nevertheless, the ability of the $\mathcal{L}_1$ control architecture to tolerate large adaptive gain implies that $\gamma_0$ can be reduced leading to overall a smaller value for $\gamma_1$. This is enabled via the low-pass system $C(s)$ in the feedback path that filters out the high-frequencies in $\bar{r}(t)$ excited by large $\Gamma_c$. The $\mathcal{L}_1$ adaptive control architecture gives a scheme for fast adaptation without generating high-frequency oscillations in the control signal.

## IV. Simulation Results

This section compares the tracking performance in the presence of pitch break and actuator failure with two adaptive control schemes: Model reference adaptive control (MRAC), which corresponds to $C(s) = 1$, and $\mathcal{L}_1$ adaptive controller. For MRAC, we reproduce the results of [16]. For the $\mathcal{L}_1$ adaptive controller we set $\omega_a = 20$, which verifies the $\mathcal{L}_1$ gain stability condition, and we set $\Gamma_c = 50000$. The performance of $\mathcal{L}_1$ controller is compared to the performance of the baseline inner-loop controller and to the performance of MRAC. The results are shown in Figures 1 and 2. For comparison purposes, simulation data are obtained from the following three closed-inner-loop systems: a) adaptation OFF, failures OFF (blue), b) adaptation OFF, failures ON (red), c) MRAC adaptation ON, failures ON (black), and d) $\mathcal{L}_1$ adaptation ON, failures ON (Magenta).

Figures 1-2 demonstrate the benefits of adaptation, when the right outboard (ROB) elevon fails at 1 second of the maneuver and the pitch break phenomenon is active throughout the entire maneuver. Figure 1 indicates that in spite of the unknown control failure and pitch break uncertainty, both MRAC and $\mathcal{L}_1$ adaptive systems are able to quickly reconfigure and track the commanded vertical acceleration, sideslip angle, roll rate, and yaw rate signals, simultaneously. In fact, Figure 1 shows that with adaptation the desired/nominal system tracking has recovered. In addition, Figure 2 compares the three virtual control feedback signals, and we have verified that no control saturation has occurred during the adaptation process. In Figure 3, the subplot of Figure 1 is re-plotted to show the perfect tracking achieved by $\mathcal{L}_1$ as compared to MRAC for vertical acceleration.

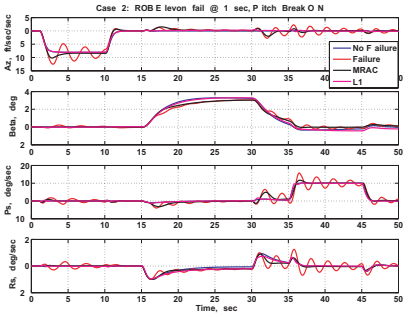


Fig. 1. Inner-Loop Adaptation with ROB Elevon Failure and Pitch Break Phenomenon: Command Tracking

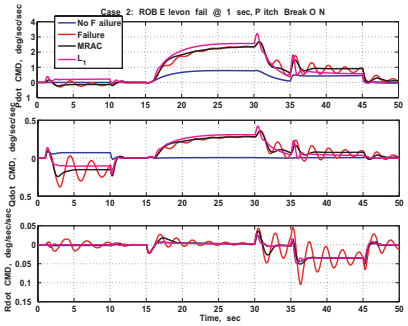


Fig. 2. Inner-Loop Adaptation with ROB Elevon Failure and Pitch Break Phenomenon: Virtual Controls

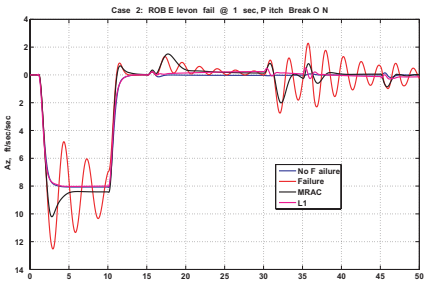


Fig. 3. Guaranteed $\mathcal{L}_1$ performance

Figure 4 demonstrates the benefits of adaptation when the inner-loop system receives repetitive vertical acceleration commands in the presence of both the ROB elevon failure and the unknown pitch break phenomenon. In [16], it has been argued that MRAC quickly dampens the oscillations caused by uncertainties and significantly reduces the corresponding control activity if repetitive commands are given to the system. However from the zoomed Figure 4 it can be seen that the repetitive command is not necessary for the $\mathcal{L}_1$

architecture, since it has guaranteed transient performance as predicted by the theory. In Figure 4, MRAC response is also plotted. For MRAC, we can see that there is small reduction in overshoot in vertical acceleration in the second pulse (20 sec time instance) as compared to the first pulse command signal (1 sec time instance).

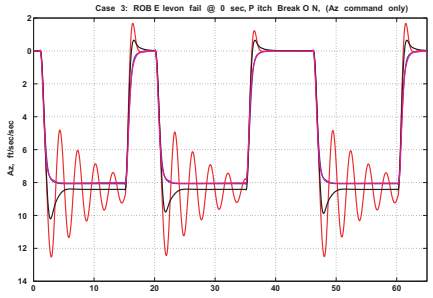


Fig. 4. $\mathcal{L}_1$ does not need repetitive commands to learn

The time-delay margin for the adaptive systems is calculated from numerical simulations by introducing the time-delay at the plant input. The time-delay margins for MRAC are summarized in Table 2. The worst case time-delay margin is 0.12 sec (the adaptive gain used in [16] for MRAC scheme is 100).

| $\dot{p}$ | $\dot{q}$ | $\dot{r}$ | |
|---|---|---|---|
| 0.16 | 0.16 | 0 | Two Loops |
| 0 | 0.13 | 0.13 | Two Loops |
| 0.17 | 0 | 0.17 | Two Loops |
| 0.12 | 0.12 | 0.12 | Three loops |

**Table 2**. Time-delay margin for MRAC

The time-delay margins for $\mathcal{L}_1$ adaptive scheme are summarized in Table 3 for the choice of $C(s) = \frac{1}{0.05s+1}$ and $\Gamma_c = 50000$. The worst case time-delay margin is $0.0425$ sec, which is smaller than the worst margin of MRAC scheme, as expected due to the addition of the filter. Now we discuss how to improve this time-delay margin via the design of $C(s)$ using the analysis from [21].

| $\dot{p}$ | $\dot{q}$ | $\dot{r}$ | |
|---|---|---|---|
| 0.0432 | 0.0432 | 0 | Two Loops |
| 0 | 0.0455 | 0.0455 | Two Loops |
| 0.05325 | 0 | 0.05325 | Two Loops |
| 0.0425 | 0.0425 | 0.0425 | Three loops |

**Table 3**. Time-delay margin for $\mathcal{L}_1$ for $C(s) = \frac{1}{0.05s+1}$

The time-delay margin for the $\mathcal{L}_1$ adaptive scheme for systems linearly dependent upon unknown parameters (i.e., in the absence of nonlinearities and RBFs), can be computed analytically as $\Gamma_c \to \infty$ [21]. In [21], $C(s)/(1 - C(s))$ appears as a multiplier in the open-loop transfer function used for calculation of the time-delay margin for the $\mathcal{L}_1$ adaptive scheme. It is obvious that one could choose $C(s)$ judiciously to maximize the phase margin of the open-loop transfer function and minimize the cross-over frequency to obtain larger time-delay margin. Towards that end, consider the following low-pass filter $C_1(s) = \frac{1}{0.05s+1}\frac{(-6s+1)^2}{(8s+1)^2}$, for which the $\mathcal{L}_1$ gain requirement holds.

The Bode plots of $C(s)$ and $C_1(s)$ are given in Figure 5. Note that a nonminimum phase filter is used to enhance the phase characteristic in the region of frequency-band in order to improve the phase margin.

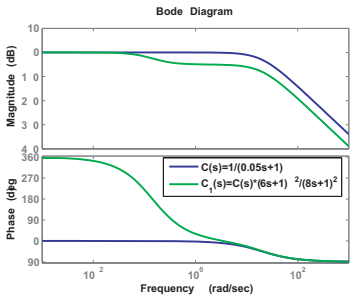


Fig. 5. Choice of $C(s)$ for maximizing the time-delay margin

The subplot of vertical acceleration of Figure 1 is repeated with $C_1(s)$ in Figure 6. We see that there is some degradation in the tracking, however it is still better than for MRAC. For this choice of $C_1(s)$, the worst case time-delay margin obtained from simulation is 0.10 sec. In Table 2, we have the worst case time-delay margin for $C(s)$ equal to 0.0425sec, which implies that $C_1(s)$ doubles the time-delay margin. Thus, improving the time-delay margin hurts the transient performance, which is consistent with the theoretical results of [19]. The worst case time-delay margin for MRAC is $0.12$, which is comparable to the worst-case margin of $C_1(s)$ in the presence of large adaptive gain $\Gamma_c = 50000$. We note that all the time-delay margins are calculated for the ROB actuator failure case and in the presence of the pitch break uncertainty.

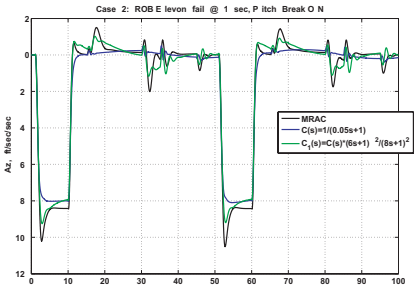


Fig. 6. Inner-Loop Adaptation with ROB Elevon Failure and Pitch Break Phenomenon: Command Tracking

However, we note that a smaller value of $\Gamma_c$ is preferable from an implementation point of view. Figure 11 shows the system response for different values of $\Gamma_c$ for both low-pass filters. It can be seen that there is almost no degradation in the time response performance. However, for the low-pass filter $C(s) = \frac{1}{0.05s+1}$, if we decrease $\Gamma_c$ from 50000

to 5000, the worst case time-delay margin decreases from 0.0425 to 0.003 (i.e. almost 14 times, much poorer than MRAC). However, for $C_1(s)$ it decreases from 0.10 to 0.07 (i.e only 1.4 times). Thus, with smaller choice of $\Gamma_c$, $C_1(s)$ is much suitable in terms of robustness as compared to $C(s)$. Table 4 summarizes the margins for $C_1(s)$ with $\Gamma_c = 5000$.

| $\dot{p}$ | $\dot{q}$ | $\dot{r}$ | |
|---|---|---|---|
| 0.09 | 0.09 | 0 | Two Loops |
| 0 | 0.09 | 0.09 | Two Loops |
| 0.12 | 0 | 0.12 | Two Loops |
| 0.07 | 0.07 | 0.07 | Three loops |

**Table 4**. Time-delay margin of $\mathcal{L}_1$ for $C_1(s)$ ( $\Gamma_c = 5000$)

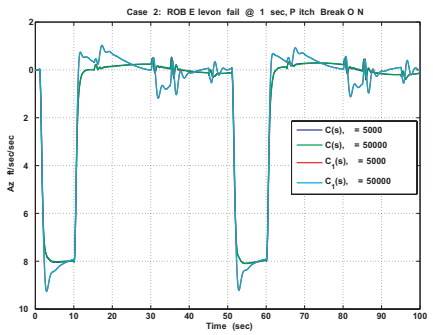


Fig. 7. Inner-Loop Adaptation with ROB Elevon Failure and Pitch Break Phenomenon: Command Tracking (for different values of $\Gamma_c$)

Finally, we simulate the system with two actuator failures to test robustness of the two adaptive control schemes towards a different class of uncertainty. Figure 8 plots the vertical acceleration command tracking in the presence of pitch break uncertainty and ROB and LMB elevon failures. We see that despite of the reasonably good time-delay margins in Table 2, MRAC loses stability, while the $\mathcal{L}_1$ adaptive control architecture retains both its tracking property and as well the worst time-delay margin of 0.07, as predicted by the $\mathcal{L}_1$ theory.

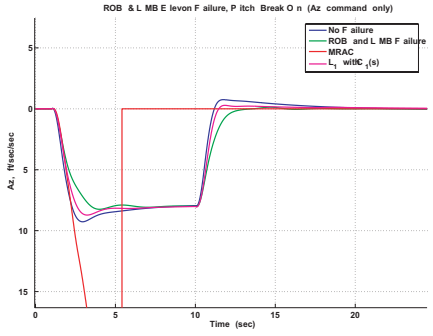


Fig. 8. MRAC loses stability in the presence of two actuator failures, while $\mathcal{L}_1$ proves guaranteed tracking

## V. Conclusion

This paper presents application of a novel $\mathcal{L}_1$ adaptive control architecture to an unstable tailless military aircraft. The robustness properties of the new architecture are compared with the conventional MRAC architecture, which show that the $\mathcal{L}_1$ adaptive controller can be designed to improve the transient command tracking and increase the robustness to time-delay.

## References


[1] Ward, D. E., Self Designing Controller, Final Report, AFRL WL-TR-97-3095, Feb. 1998.

[2] Urnes-Jr., J. E., NASA F-15 Intelligent Flight Control, Final Report, Boeing Report No. STL 99P0040, May 1999.

[3] Wise, K. A,., Reconfigurable Systems for Tailless Fighter Aircraft - RESTORE, Final Report, AFRL-VA–WP-TR-99-3067.

[4] Kim, B.S., Calise, A.J., Nonlinear Flight Control Using Neural Networks, J. of Guidance, Contr. and Dynamics, 52(1):26-33, 1997.

[5] Wise, K., and Brinker, J., Reconfigurable Flight Control for a Tailless Advanced Fighter Aircraft, AIAA 98-4107, AIAA GNC Conf., 1998.

[6] Wise, K., Brinker, J., Calise, A., Enns, D., Elgersma, M., Voulgaris, P., Direct Adaptive Reconfigurable Flight Control For A Tailless Advanced Fighter Aircraft, Int. J. of Robust Nonlinear Contr., 9:999-1012, 1999.

[7] Brinker, J., Wise, K. A. Flight Testing of a Reconfigurable Flight Control Law on the X-36 Tailless Fighter Aircraft, AIAA-2000-3941, AIAA GNC Conf., 2000.

[8] McFarland, M., Calise, A., Neural-adaptive nonlinear autopilot design for an agile anti-air missile, AIAA 96-3914, AIAA GNC Conf., 1996.

[9] McFarland, M., Calise, A., Multi-layer Neural networks and adaptive nonlinear control of for agile anti-air missiles, AIAA 97-3540, AIAA GNC Conf., 1997.

[10] Sharma, M., Calise, A. J., Corban, J. E. Application of an Adaptive Autopilot Design to a Family of Guided Munitions, AIAA 2000-3969, AIAA GNC Conf., 2000.

[11] Sharma, M., Calise, A. Neural Network augmentation of Existing Linear Controllers, AIAA 2001-4163, AIAA GNC Conf., 2001.

[12] Corban, J., Burkemper, V., Holt, K., Evers, J., Calise, A., Sharma, M. Flight Test of an Adaptive Autopilot For Precision Guided Munitions, AIAA Missile Sciences Conf., 2002.

[13] Sharma, M., Lavretsky, E., Wise, K., Application and Flight Testing of an Adaptive Autopilot on Precision Guided Munitions, AIAA 2006-6568, AIAA GNC Conf., 2006.

[14] Wise, K., Lavretsky, E., Zimmerman, J., Francis-Jr., J., Dixon, D., Whitehead, B., Adaptive Flight Control of a Sensor Guided Munition. AIAA 2005-6385, AIAA GNC Conf., 2005.

[15] Steinberg, M., Historical Overview of Research in Reconfigurable Flight Control, Proceedings of the Institution of Mechanical Engineers. Part G: J. of Aerospace Eng., 219:263-275, 2005.

[16] Lavretsky, E. Wise, K., Adaptive Flight Control for Manned/Unmanned Military Aircraft, Amer. Contr. Conf., 2005.

[17] Wise, K., Lavretsky, E., Hovakimyan, N., Adaptive Control of Flight: Theory, Applications and Open Problems, Amer. Contr. Conf., 2006.

[18] Cao, C., Hovakimyan, N., Design and Analysis of a Novel $\mathcal{L}_1$ Adatpive Control Architecture, Part I: Control Signal and Asymptotic Stability. Amer. Contr. Conf., pp. 3397-3402, 2006.

[19] Cao, C., Hovakimyan, N., Design and Analysis of a Novel $\mathcal{L}_1$ Adatpive Control Architecture, Part II: Guaranteed Transient Performance. Amer. Contr. Conf., pp. 3403-3408, 2006.

[20] Cao, C., Hovakimyan, N. Guaranteed transient performance with $\mathcal{L}_1$ adaptive controller for systems with unknown time-varying parameters: Part I. Amer. Contr. Conf., 2007.

[21] Cao, C., Hovakimyan, N., Stability Margins of $\mathcal{L}_1$ Adaptive Control Architecture, Amer. Contr. Conf., 2007.

[22] Cao, C., Hovakimyan, N., Novel $\mathcal{L}_1$ neural network adaptive control architecture with guaranteed transient performance. IEEE Trans. Neural Networks, 18(4), 2007.

[23] Wise, K., Bank-To-Turn Missile Autopilot Design Using Loop Transfer Recovery, J. Guidance, Contr. and Dynamics, 13(1):145-152, 1990.

[24] Wise, K., Brinker, J. S., Linear Quadratic Flight Control For Ejection Seats, J. Guidance, Contr. and Dynamics, 19(1):15-22, 1996.

[25] Wise, K., Deylami, F., Approximating a Linear Quadratic Missile Autopilot Design Using an Output Feedback Projective Control, AIAA 91-2613, AIAA Guidance, Navigation, and Contr. Conf., 1991.

[26] Pomet, J., Praly, L., Adaptive Nonlinear Regulation: Estimation from Lyapunov Equation. IEEE Trans. Autom. Contr., 37(6):729-740, 1992.